Integrated Pico-Tesla Resolution Magnetoresistive Sensors for Miniaturised Magnetomyography

Siming Zuo, *Student Member, IEEE*, Kianoush Nazarpour, *Senior Member, IEEE*, Tim Böhnert, Elvira Paz, Paulo Freitas, *Senior Member, IEEE*, Ricardo Ferreira, *Member, IEEE* and Hadi Heidari, *Senior Member, IEEE*

***Abstract*—Magnetomyography (MMG) is the measurement of magnetic signals generated in the skeletal muscle of humans by electrical activities. However, current technologies developed to detect such tiny magnetic field are bulky, costly and require working at the temperature-controlled environment. Developing a miniaturized, low cost and room temperature magnetic sensors provide an avenue to enhance this research field. Herein, we present an integrated tunnelling magnetoresistive (TMR) array for room temperature MMG applications. TMR sensors were developed with low-noise analogue front-end circuitry to detect the MMG signals without and with averaging at a high signal-to-noise ratio. The MMG was achieved by averaging signals using the Electromyography (EMG) signal as a trigger. Amplitudes of 200 pT and 30 pT, corresponding to periods when the hand is tense and relaxed, were observed, which is consistent with muscle simulations based on finite-element method (FEM) considering the effect of distance from the observation point to the magnetic field source.**

I. Introduction

Detecting weak biomagnetic fields, Magnetomyography (MMG), first formally proposed in 1972 by Cohen and Gilver [1]. With the development of efficient magnetic technologies, this non-invasive technique becomes more attractive because it has great potential to improve medical diagnosis and health monitoring, and to develop rehabilitation robotics where the human-machine interface can assist the disabled with limb difference to perform essential activities of daily living [2]. The MMG signals are recorded as components of the magnetic field vector versus time, which is generated the action potential from electric currents travelling along with skeletal muscle fibres. Compared with a well-established Electromyography (EMG) method, the MMG measurement has become an effective alternative means due to its significantly higher spatial resolution despite the same temporal resolution as the EMG signals [3]. Both signals are directly from the Maxwell-Ampère law, shown in Fig. 1. The magnitude of magnetic field reduces significantly with the distance between the origin and the sensor, thereby with MMG spatial resolution is uplifted [4]. In addition, the non-invasive MMG offer vector information of the muscle movement, long-term biocompatibility with tissue, a higher signal-to-noise, and better positioning and fast screening of sensors without electric contacts [3], [5]–[8]. State-of-the-art EMG measurements are even using needle recording probes, which is possible to accurately assess muscle activity but painful and limited to tiny areas with poor spatial sampling points [9]. Moreover, magnetic sensors with biocompatible materials can be fully packaged to form a miniaturized implantable system [10].

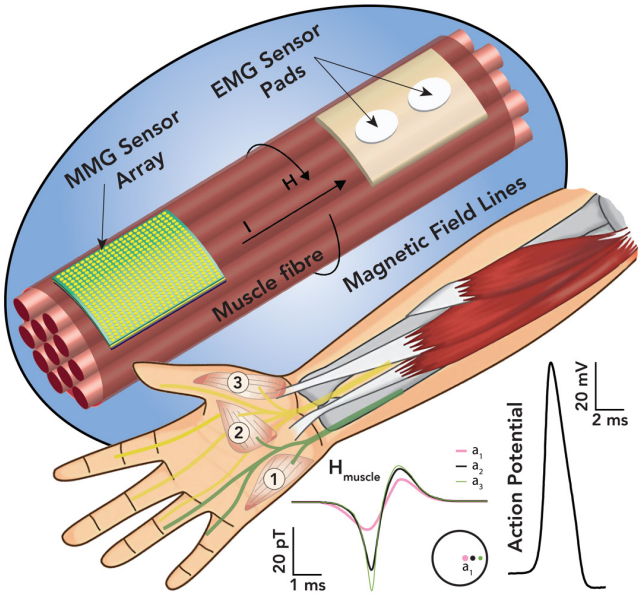

Fig. 1. Schematic of the magnetic versus electric approaches to sensing muscle activity with the typical hand muscle location. 1) M. abductor digiti; 2) Several intrinsic muscles of thumb; 3) M. abductor pollicis.

However, detecting ultra-low MMG signals is not an easy task. Compared with the magnitude of the EMG signal in the scale of milli-volts, the MMG signal is extremely small and just in the range of pico (10^{-12}) to femto (10^{-15}) Tesla [11], decreasing with the distance between the measurement point and the skeletal muscle. Currently, the most common approach is utilizing superconducting quantum interference devices (SQUIDs). They led the development of the MMG until now since it is the most sensitive device so far with the femto-Tesla detection ability, and possibly achieve atto-Tesla detection with averaging [12]. Nevertheless, their high cost, bulky weight and operation at the low-temperature environment limit the spread of these techniques. As time goes by, optimally-pumped magnetometers (OPMs) from QuSpin Inc. have been performed in the MMG study [13], [14]. The new generation of OPM offers small physical size with significantly improved limit-of-detection below 100 fT/√Hz. Unfortunately, it is still rather complex for the sensor setup with proper operation. Current experiments based on SQUIDs and OPMs for MMG sensing are conducted in heavily shielded rooms, which are

This work was supported by grant EP/R511705/1 from EPSRC, UK. The work of KN is supported by grants EP/N023080/1 and EP/R004242/1 from EPSRC, UK.

S. Zuo and H. Heidari are with the Microelectronics Lab, James Watt School of Engineering, University of Glasgow, G12 8QQ, UK. (e-mail: z.siming.1@research.gla.ac.uk and Hadi.Heidari@glasgow.ac.uk).

K. Nazarpour is with the School of Engineering and the Biosciences Institute, Newcastle University, Newcastle upon Tyne NE1 7RU, U.K. (e-mail: kianoush.nazarpour@newcastle.ac.uk).

T. Böhnert and R. Ferreira are with the INL, International Iberian Nanotechnology Laboratory, Av. Mestre Jose Veiga s/n, 4715-330 Braga, Portugal. (e-mail: tim.boehnert@inl.int and ricardo.ferreira@inl.int).

Authorized licensed use limited to: Middlesex University. Downloaded on October 20,2020 at 07:44:29 UTC from IEEE Xplore. Restrictions apply.

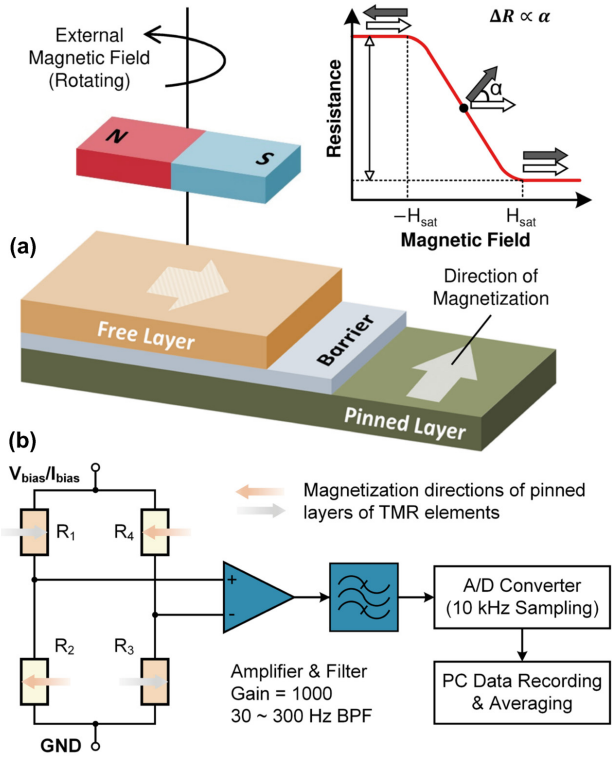

Fig. 2. Schematic diagrams of (a) TMR structure and its transfer curve and (b) Biomagnetic field measurement system using four TMR sensors. the signal is input to the amplifier circuit, and the analogue-to-digital converted data recorded and averaged using PC software. BPF: bandpass filter.

expensive and bulky for a daily basis. As a consequence, a miniaturised, highly sensitive, low-cost and low-power MMG system must be fulfilled to perform at room temperature. We have previously demonstrated a high-performance Hall sensor in CMOS technology with its integrated readout circuit [2]. However, the Hall sensors require a highly stable DC power supply to excite the Hall effect and a complex interface circuit to process collected weak Hall voltages under surrounding noise [15]. However, spintronic sensors [16], especially our previous structure of the tunnel magnetoresistance (TMR) sensors [17], offer high sensitivity than giant magnetoresistive (GMR) sensors for weak magnetic field sensing. Recent spintronics-based MMG measurement was carried out by the GMR sensor [8]. Its detection limit of 3.5 nT cannot meet the requirement of the surface measurement (pico-Tesla level).

II. Tunnelling Magnetoresistive Sensor

A. Structure and Principle

The TMR effect occurs in a nanoscale magnetic tunnel junction where electrons can tunnel through very thin ordinary insulating materials under the proper conditions. The basic TMR structure and its transfer curve are illustrated in Fig. 2(a). It consists of free layer/barrier/pinned layers corresponding to ferromagnetic (FM)/insulating/FM materials. Applying a bias voltage or current to the TMR sensor, its electrical resistance changes as a linear function of the magnetic field strength over a certain field range due to the dependence of the tunnelling probability on relative magnetization orientations in two FM layers. The largest (R_{AP}) and lowest (R_P) resistance values are obtained when the FM layers have antiparallel and parallel orientations respectively. For an ideal TMR sensor, its transfer curve is linear and hysteresis-free. Saturation fields (H_{sat}) define the ideal linear range ($2H_{sat}$) of the device. The sensor sensitivity that represents how reactive the sensor is to a field variation can be measured experimentally from the slope of the transfer curve. However, the noise level will determine the limit of detection. The field noise spectral density in the $1/f$ dominated regime of N TMR sensors can be expressed as

$$S_H^{1/f} = \frac{S_V}{dV/(\mu_0 dH)} = \left(\frac{1}{R_N}\frac{dR_N}{\mu_0 dH}\right)^{-1}\sqrt{\frac{\alpha}{NA_1}\frac{1}{f}} \qquad (1)$$

where dR_N/dH is the sensor sensitivity, μ_0 is the vacuum permeability of free layer, α is the Hooge's parameter, N is the number of sensors in series and A_1 is the area of each individual sensor. Thus, to minimize the low-frequency noise, the total sensing area NA_1 must be maximized.

In addition, the field noise spectral density in the white noise regime of N TMR sensors is defined as follows

$$S_H^{White} = \left(\frac{1}{R_N}\frac{dR_N}{\mu_0 dH}\right)^{-1}\sqrt{\frac{2e}{I_N}coth\left(\frac{eV_N}{2K_BT}\right)} \qquad (2)$$

where e is the charge of the electron, I_N is the DC current, V_N is the dc bias voltage across the tunnel junction, K_B is the Boltzmann's constant and T is the temperature. To minimize the high-frequency noise, the total resistance (R_N) must be minimized and dR_N/dH must be maximized. Therefore, from eq. (1) and (2), the best overall noise performance is obtained with large arrays of large area sensors.

B. Sensor Characteristic

The schematic diagram of the MMG measurement system operated at room temperature is shown in Fig. 2(b). A full Wheatstone bridge structure is utilized to compensate thermal drift, which including two types of TMR elements with opposite sensing directions by setting magnetizations between the pinned layer and free layer in 90º (R_1, R_3) and –90º (R_2, R_4) respectively [18]. The output voltage of the bridge was input to an amplifier circuit based on AD8429 (Analog Devices, Inc) After a 1000 gain amplification, the signal was passed through an 8th-order Butterworth bandpass filter of 30 to 300 Hz.

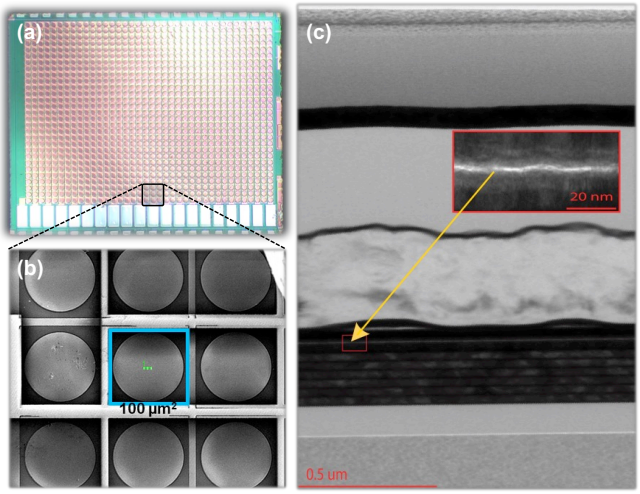

Fig. 3. (b) A microscope image; (c) Enlarged image with a size of 100 μm² per TMR element; (d) TEM image of the entire stack structure where the red box shows indication of MgO barrier surrounded by Fe:Co matrix.

Authorized licensed use limited to: Middlesex University. Downloaded on October 20,2020 at 07:44:29 UTC from IEEE Xplore. Restrictions apply.

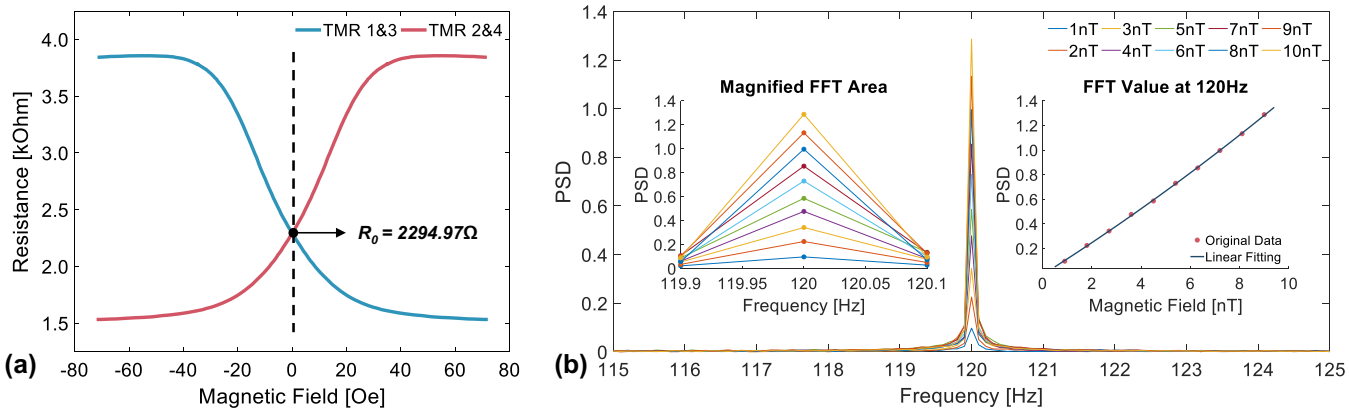

Fig. 4. (a) Measured resistances variation of the TMR sensor with magnetic fields; (b) The MMG system response in a frequency domain.

Finally, a 24-bit analogue-to-digital converter with a sampling rate of 10 kHz is used for data acquisition and further analysis.

To minimize $1/f$ noise of the sensor [19], 1102 TMR elements are connected in 58 series and 19 parallel (Fig. 3a). The size of each TMR sensor is 100 × 100 µm (Fig. 3b) while electronic pads are 200 × 400 µm and separated by 250 µm. The TMR stack consists of (unit: nm) [5 Ta / 25 CuN] × 6 / 5 Ta / 5 Ru / 20 IrMn / 2 $CoFe_{30}$ / 0.85 Ru / 2.6 $CoFe_{40}B_{20}$ / MgO [9 kΩ·µm^2] / 2 $CoFe_{40}B_{20}$ / 0.21 Ta / 4 NiFe / 0.20 Ru / 6 IrMn / 2 Ru / 5 Ta / 10 Ru. Fig. 3(c) illustrates entire stack structure by a transmission electron microscope. The bottom NiFe and CoFeB free layers show anti-ferromagnetic coupling where the magnetization reversal process reflects that of the thick NiFe layer [17]. In addition, an annealing process was performed after micro-fabrication to ensure that orthogonal magnetic axes of the free and pinned layers were aligned [20].

Both sensor characteristics and MMG measurements were carried out in a shielded chamber with a residual magnetic field of 4 nT to counteract the influence of external magnetic fields. Setting a driving current of the Wheatstone bridge to be 20 mA, the measurement result is shown in Fig. 4(a). The linear range of the sensor is about from −1 Oe to 1 Oe. The average R×A is 9 kΩ·µm^2 with 13% uniformity and the TMR ratio is 152% with 9% uniformity. For the full bridge setup, the measured voltage change of each TMR element is 280 Ω·µm^2/Oe and the sensitivity is measured as ~ 0.617 V/Oe. Taking magnetic signals at a specific frequency of 120 Hz for example, Fig. 4(b) illustrates the power spectral density (PSD) in which has the MMG system has a very linear response in a frequency domain by a fast Fourier transform.

III. Muscle Modelling and Simulation

To validate the proposed system, finite-element method (FEM) simulations were performed in *COMSOL*. Fig. 5(a) illustrates the experimental setup. An active compensation technique, consisting of a geomagnetic field cancellation box with an array of tri-axial square Helmholtz coils and double stainless-steel tubes, was employed to reduce noise sources such as the acoustic noise and disturbances of magnetic and electric fields from the earth and surrounding equipment. In addition, a compact muscle model based on its actual structure was investigated. The parameters to describe the muscle bundle such as the radius, thickness and conductivity were adopted from the literature [21]. From simulation results in 3D (Fig. 5b) and 2D (Fig. 5c), it shows that the total ring magnetic

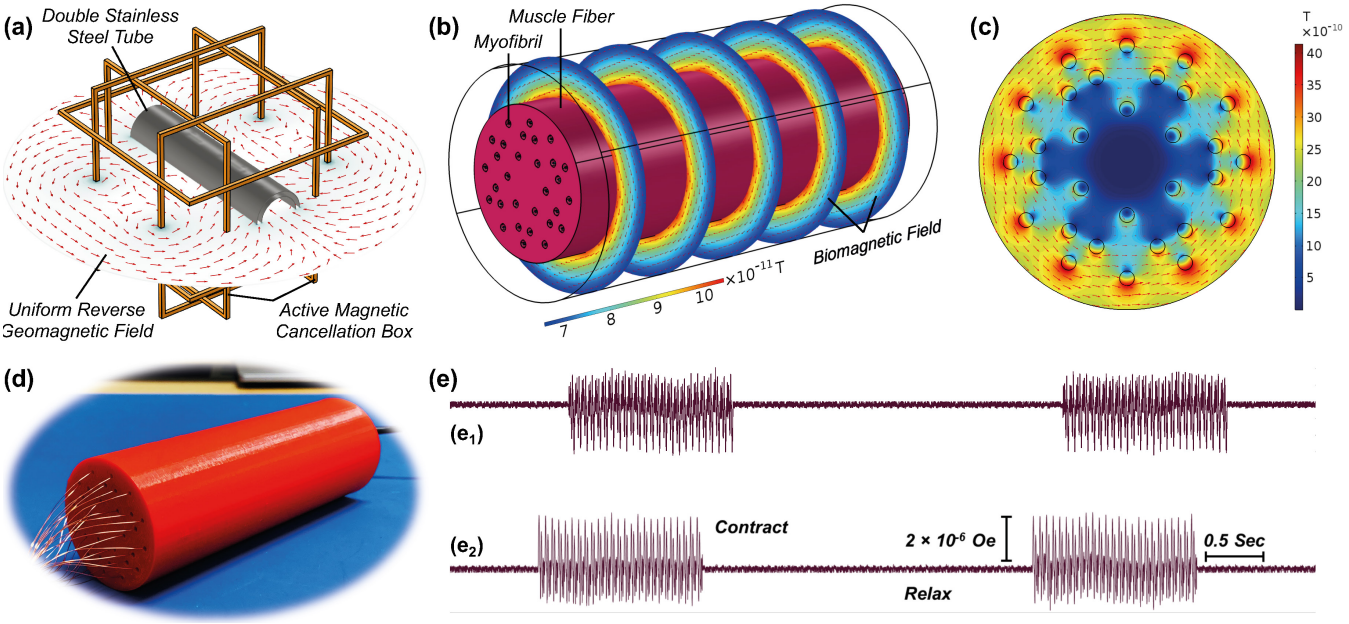

Fig. 5. (a) Measurement setup; (b) *COMSOL* 3D finite-element simulation results of biomagnetic fields generated from the muscle fibre; (c) 2D results with muscle fibre and myofibrils; (d) 3D printed flexible muscle with a group of fibres; (e) measured magnetic fields from the 3D printed muscle model.

Authorized licensed use limited to: Middlesex University. Downloaded on October 20,2020 at 07:44:29 UTC from IEEE Xplore. Restrictions apply.

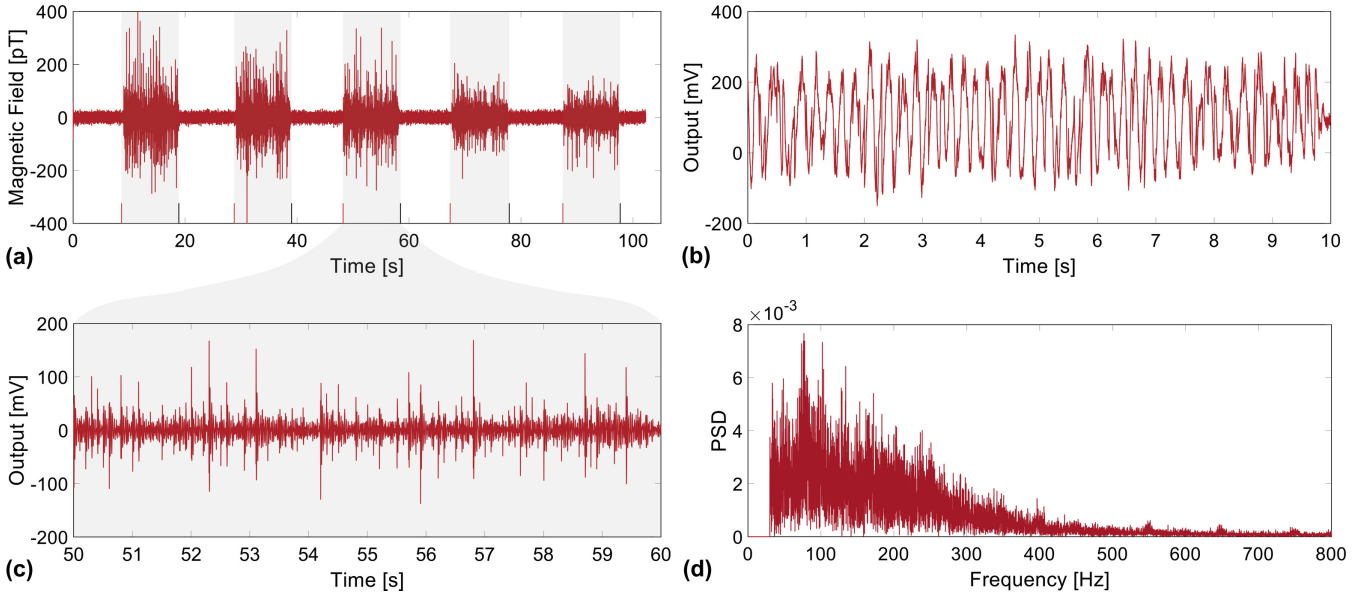

Fig. 6. (a) Measured MMG signals (100s) from the proposed TMR system when the hand muscles were relaxed and tense respectively; (b) Raw MMG signals without filtering when the hand muscles were in the tense state; (c) MMG signals after a 20th-order bandpass (30 - 300Hz) Butterworth filter; (d) Power spectrum from the tense hand muscles.

field is the superposition of each muscle fibre where nano to pico-Tesla range fields will be generated. The red arrows and colour legend show the direction and magnitude of magnetic fields respectively. Moreover, a 3D printed muscle model (Fig. 5d) with an enlarged size was created to verify the simulations. Finally, measured magnetic fields on the surface of the muscle fibre are shown in Fig. 5(e). Signals of contract and relax states were measured continuously. In time series, there is a clear difference between them. An approximate amplitude of 200 pT signals corresponds to the period of hand contraction, while the amplitude of the noise activity was also recorded, corresponding to the relaxed hand.

IV. Implementation And Experimental Results

Surface EMG signals were recorded by a 3-lead MyoWare wearable muscle system (Advancer Technologies, LLC) with the MMG signals at the same time as an effective reference. Both the TMR sensor array and EMG electrode were exactly placed on the skin of abductor pollicis brevis hand muscle to detect the transverse component of the magnetic field and electric potential in a healthy male subject (aged 24 years), who volunteered for the study and signed informed consent. The subject is right-handed and has no severe somatic diseases and any mental or neurological diseases. The Institution's Ethical Review Board approved all experimental procedures involving human subjects. Then, both sensing systems were prepared and tested individually with a data acquisition system (EVAL-AD7177-2, Analog Devices, Inc).

The 100-second MMG signals from the proposed TMR system were recorded and analyzed at the room temperature to verify the whole process of muscle activities. As shown in Fig .6(a), it was a clear difference in time series between when the hand was tense and when the hand was relaxed. The first type is a time-domain with an amplitude of 200 pT, corresponding to periods when the hand is tense. This amplitude of the MMG signals corresponds to the accepted ideas about the magnetic field of skeletal muscles. The second type is a time-domain with an amplitude of 20 to 30 pT, corresponding to the lengths of time when the hand is relaxed. This amplitude is roughly equal to the amplitude of the noise activity records in a relaxed hand. Without filtering, the raw MMG signal from the tense muscles is illustrated in Fig. 6(b), which include wideband noise and movement artifacts. Nevertheless, by using the 20th-order bandpass Butterworth filter of 30 to 300Hz (Fig. 6c), the signals not only became clearer but also confirmed that the positions of the peaks for both the MMG and EMG were almost the same. The approximate amplitude of 200 pT was observed, which is consistent with the reported value measured by SQUIDs [11]. Finally, the MMG power spectrum is shown in Fig. 6(d) with a wideband frequency range, in which the MMG signals of the tensed hand state is many times greater than noise. At frequencies from 30 to 300 Hz, the signal-to-noise ratio is greater than 20.

V. Conclusion and Future Work

In summary, we showed the first result of highly sensitive TMR-recorded ultra-low MMG signals from the human hand muscle at room temperature. As an effective alternative to SQUIDs, this new method demonstrates the viability of the miniaturized TMR sensor for medical and biological research at a safe manner. By combining both electrical and magnetic sensors, we can distinguish different signals based on complementary information from the muscle activities, which is targeted, repeatable and safe. The test subject strained and relaxed the hand muscle in a magnetically shielded box and double stainless-steel chambers. The MMG recording was achieved by using the EEG signal as a trigger. An amplitude of 200 pT was observed in a wide frequency band with the SNR over 20. In addition, the FEM simulations and 3D printed compact muscle model were investigated to validate the experimental results. The future multi-channel and real-time measurements with a flexible TMR sensor array and on-chip magnetic background noise cancellation may lead to further improvements in simplification and miniaturization of the MMG system and reduce the cost.

Authorized licensed use limited to: Middlesex University. Downloaded on October 20,2020 at 07:44:29 UTC from IEEE Xplore. Restrictions apply.

REFERENCES

[1] D. Cohen and E. Givler, 'Magnetomyography: Magnetic fields around the human body produced by skeletal muscles', *Appl. Phys. Lett.*, vol. 21, no. 3, pp. 114–116, 1972.

[2] H. Heidari, S. Zuo, A. Krasoulis, and K. Nazarpour, 'CMOS Magnetic Sensors for Wearable Magnetomyography', in *40th International Conference of the IEEE Engineering in Medicine and Biology Society*, pp. 2116–2119, 2018.

[3] K. K. Parker and J. P. Wikswo, 'A model of the magnetic fields created by single motor unit compound action potentials in skeletal muscle.', *IEEE Trans. Biomed. Eng.*, vol. 44, no. 10, pp. 948–957, 1997.

[4] S. Zuo, H. Heidari, D. Farina, and K. Nazarpour, 'Miniaturized magnetic sensors for implantable magnetomyography', *Adv. Mater. Technol.*, 2020. doi:10.1002/admt.202000185.

[5] T. Masuda, H. Endo, and T. Takeda, 'Magnetic fields produced by single motor units in human skeletal muscles', *Clin. Neurophysiol.*, vol. 110, no. 3, pp. 384–389, 1999.

[6] K. Tsukada and T. Kiwa, 'Noninvasive measurements of magnetic field generated by induced current within human body under exposure to very low frequency electromagnetic fields', *Jpn. J. Appl. Phys.*, vol. 44, no. 4L, p. L532, 2005.

[7] R. S. Wijesinghe, 'Detection of magnetic fields created by biological tissues', *J. Electr. Electron.*, vol. 3, no. 1, p. 1, 2014.

[8] F. Barbieri *et al.*, 'Local recording of biological magnetic fields using Giant Magneto Resistance-based micro-probes', *Sci. Rep.*, vol. 6, p. 39330, 2016.

[9] K. Woeppel, Q. Yang, and X. T. Cui, 'Recent advances in neural electrode–tissue interfaces', *Curr. Opin. Biomed. Eng.*, vol. 4, pp. 21–31, 2017.

[10] K. Nazarpour, A. R. Sharafat, and S. M. P. Firoozabadi, 'Application of higher order statistics to surface electromyogram signal classification', *IEEE Trans. Biomed. Eng.*, vol. 54, no. 10, pp. 1762–1769, 2007.

[11] M. A. C. C. Garcia and O. Baffa, 'Magnetic fields from skeletal muscles: A valuable physiological measurement?', *Front. Physiol.*, vol. 6, no. Aug, pp. 1–4, 2015.

[12] R. L. Fagaly, 'Superconducting quantum interference device instruments and applications', *Rev. Sci. Instrum.*, vol. 77, no. 10, p. 101101, 2006.

[13] P. J. Broser *et al.*, 'Optically pumped magnetometers for magneto-myography to study the innervation of the hand', *IEEE Trans. Neural Syst. Rehabil. Eng.*, vol. 26, no. 11, pp. 2226–2230, 2018.

[14] G. Z. Iwata *et al.*, 'Biomagnetic signals recorded during transcranial magnetic stimulation (TMS)-evoked peripheral muscular activity', *arXiv Prepr. arXiv1909.11451*, 2019.

[15] H. Heidari, E. Bonizzoni, U. Gatti, and F. Maloberti, 'A CMOS current-mode magnetic hall sensor with integrated front-end', *IEEE Trans. Circuits Syst. I Regul. Pap.*, vol. 62, no. 5, pp. 1270–1278, 2015.

[16] P. P. Freitas, R. Ferreira, and S. Cardoso, 'Spintronic Sensors', *Proc. IEEE*, vol. 104, no. 10, pp. 1894–1918, 2016.

[17] S. Zuo, K. Nazarpour, and H. Heidari, 'Device Modeling of MgO-Barrier Tunneling Magnetoresistors for Hybrid Spintronic-CMOS', *IEEE Electron Device Lett.*, vol. 39, no. 11, pp. 1784–1787, 2018.

[18] S. Zuo, H. Fan, K. Nazarpour, and H. Heidari, 'A CMOS Analog Front-End for Tunnelling Magnetoresistive Spintronic Sensing Systems', in *IEEE International Symposium on Circuits and Systems (ISCAS)*, pp. 1-5, 2019.

[19] M. D. Cubells-Beltrán, C. Reig, D. R. Muñoz, S. I. P. C. de Freitas, and P. J. P. De Freitas, 'Full wheatstone bridge spin-valve based sensors for IC currents monitoring', *IEEE Sens. J.*, vol. 9, no. 12, pp. 1756–1762, 2009.

[20] E. Paz, R. Ferreira, and P. P. Freitas, 'Linearization of Magnetic Sensors With a Weakly Pinned Free-Layer MTJ Stack Using a Three-Step Annealing Process', *IEEE Trans. Magn.*, vol. 52, no. 7, pp. 1–4, 2016.

[21] N. Ganapathy, J. W. Clark Jr, and O. B. Wilson, 'Extracellular potentials from skeletal muscle', *Math. Biosci.*, vol. 83, no. 1, pp. 61–96, 1987.

Authorized licensed use limited to: Middlesex University. Downloaded on October 20,2020 at 07:44:29 UTC from IEEE Xplore. Restrictions apply.